

Determination of mechanical and vibration properties of SiO₀₀₁, SiO₁₁₀, SiO₁₁₁ nanowires using first principles approach

A. Wesam Al-Mufti ^a, Th. S. Dhahi ^b, Alaa Kamal Yousif Dafhalla ^c, Jawaher Suliman Altamimi ^d, Duria Mohammed Ibrahim Zayan ^d, Azath Mubarakali ^e, Abdulrahman Saad Alqahtani ^f, Mohamed Elshaikh Elobaid ^g, Tijjani Adam ^{g,i,j,k} *, M. N. Afnan Uda ^h, M. N. A. Uda ⁱ, Subash Chandra Bose Gopinath ^{i,j,k}, and U. Hashim ^l

^aDepartment of Medical Physics, College of Science, Al-Karkh University of Science, Baghdad, Iraq

^bHealth and Medical Technicals College, Southern Technical University Basrah, Iraq

^cDepartment of Computer Engineering, College of Computer Science and engineering, University of Ha'il, Kingdom of Saudi Arabia

^dDepartment of Computer Science, Najran University, Kingdom of Saudi Arabia

^eDepartment of Informatics and Computer Systems, College of Computer Science, King Khalid University, Abha, Kingdom of Saudi Arabia

^fCollege of Computing and Information Technology, University of Bisha, Kingdom of Saudi Arabia

^gFaculty of Electronic Engineering & Technology, Universiti Malaysia Perlis, 02600 Arau, Perlis, Malaysia

^hFakulti Kejuruteraan, Universiti Malaysia Sabah, 88400 Kota Kinabalu, Sabah, Malaysia

ⁱFaculty of Chemical Engineering & Technology, Universiti Malaysia Perlis, 02600 Arau, Perlis, Malaysia

^jInstitute of Nano Electronic Engineering, Universiti Malaysia Perlis, 01000 Kangar, Perlis, Malaysia

^kMicro System Technology, Centre of Excellence (CoE), Universiti Malaysia Perlis, 02600 Arau, Perlis, Malaysia

^lElectrical & Electronics Engineering Programme, Faculty of Engineering, Universiti Malaysia Sabah, 88400 Kota Kinabalu, Sabah, Malaysia

*Corresponding author. Tel.: +6-011-2515-5077; e-mail: tijjani@unimap.edu.my

Received 22 September 2023, Revised 15 August 2024, Accepted 24 August 2024

ABSTRACT

Nanowires play an important role in various applications, especially in exploring their electronic properties. While their mechanical properties have also demonstrated potential, they have not yet been fully theoretically investigated to determine their specific mechanical properties. The goal of this study is to investigate the mechanical properties of SiO nanowires using density functional theory and a first-principles approach. The mechanical properties along (001), (110), and (111) orientations were examined. The strains of 0.1164×10^{-5} , 0.12×10^{-5} , and 0.115×10^{-5} for each of the three orientations, with moduli of 149.5 GPa, 75.5 GPa, and 85.1 GPa, were found. The total energies along the same orientations (001), (110), and (111) were found to be -1.33, -1.35, and -1.37 eV, respectively. The corresponding Debye temperatures were 676.14 K, 454.70 K, and 616.26 K. The values of Frantsevich's ratios of 0.38, 0.22, and 0.36 along with Poisson's ratios of 0.33, 0.40, and 0.34 confirmed that the nanowires in all crystal directions are ductile. These results demonstrate that the first-principles approaches utilised in this study to study SiO nanowires' characteristics were able to capture the exact behavior of the nanowire parameters.

Keywords: Nanowire size, Nanowire orientation, Electronic properties, Mechanical properties, Silicon nanowire

1. INTRODUCTION

Nanowires have wide applications in advanced materials, biotechnology, electronic technology, photology, and so forth. Studying and controlling the mechanical behaviour of nanowires is of great significance. Nanowires are often observed to be size-dependent, owing to their nanoscale size [1]. Compared to their bulk counterparts, nanowires frequently exhibit extraordinary strength. The increased strength is ascribed to the decreased quantity of structural flaws and displacements, in addition to the lack of grain boundaries within the extended, uninterrupted structure. When subjected to stress, nanowires with high elasticity can flex and revert to their former shape. This characteristic is essential for applications that call for materials resistant to repeated mechanical deformation, nanowires are very sturdy despite their small size. Defects, crystal structure, and material composition are some of the variables that

affect this stiffness. Due to the potential of regulating devices with smaller dimensions, nanotechnology has lately drawn the interest of various researchers working in this area [2]. This possibility has attracted greater interest. By enabling the production and use of a variety of structures and geometries, technology has enabled the establishment of various new options for defining the fundamental behaviour of devices [3–5]. The structure may be created and constructed from the top down or the bottom up [6–9]. Additionally, the method has facilitated the fabrication of novel nanostructures for a range of applications. It has opened up two distinct avenues: nanodevices and nanomaterials. The result of modifying the atomic arrangement offers enormous opportunities for the development of unique nanomaterials that are not possible in the conventional sense [10]. The most popular and advanced technique is the first-principles approach, which does not depend on experimental data to determine the

genuine and reliable behaviour of the device. This is achievable because the atomic arrangement imparts a whole new appearance to the structure, and the geometries affecting the device's mechanical characteristics are readily identifiable [11]. Numerous research has shown the feasibility of conducting controlled experiments on molecular-scale SiO nanowires utilising an array and orientation with a very small diameter [12]. When materials' diameters are lowered to the nanoscale, their mechanical properties become more sensitive to a variety of causes and circumstances [13]. The mechanical sensitivity of nanowires is related to their size, shape, and orientation, as revealed by the researchers [14]. Numerous researchers [7] have thoroughly investigated the influence of these parameters on the mechanical properties of silicon nanowires experimentally, but the degree to which these variables exist theoretically remains an open subject [15]. In terms of silicon shape, many researchers [3] argued that circular cross-sections are more resistant to strain than square cross-sections; hence, this study is important for better understanding circular nanowires and verifying past results [16]. This is because the full force will be distributed uniformly throughout the N atom chains that make up the nano rod's cross-section [17]. Strain and stress are critical mechanical qualities; strain is defined as the ratio of the change in Several predictions about the mechanical characteristics of macroscopic silicon structures have been obtained using density functional theory. A certain amount of brittleness may be present in some nanowires, especially those composed of brittle materials. The mechanical characteristics of nanowires are mostly dependent on their size; however, their small size can result in unusual failure processes and, in some situations, increased ductility as compared to bulk materials. Mechanical behavior is influenced by quantum effects, which grow more pronounced as the nanowire size decreases. For instance, the local density approximation (LDA) model in combination with the generalised gradient approximation (GGA) model indicates that size influences mechanical characteristics [18-23]. As a result, more investigation is advised. Theoretically, by using density functional theory (DFT) to determine the mechanical properties of silicon nanowires, ABINIT was utilised in conjunction with MATLAB to construct an interaction between various mechanical parameters such as modulus, strain, and stress. The mechanical properties of nanowires can be greatly influenced by their enormous surface-to-volume ratio. In comparison to bulk materials, surface effects can result in modified deformation mechanisms, increased hardness, and different fracture behavior. Nanowires can also show distinctive thermal behavior. Thermal variations can have a more noticeable impact on the mechanical response of a material at the nanoscale. Comprehending and adjusting these mechanical characteristics is essential for customizing nanowires for particular uses, including in energy storage, sensors, nanoelectronics, and other domains linked to nanotechnology. Thus, the aim of the study is to determine the mechanical and vibration properties of SiO₀₀₁, SiO₁₁₀, and SiO₁₁₁ nanowires using the first principles approach which is vital in applications such surface modification.

2. COMPUTATIONAL METHODS FOR DETERMINING NANOWIRE MECHANICAL PROPERTIES

Strain is defined as a change in form or size, and mechanical attributes are determined using mechanical characteristics. Hooke's law states that stress is proportional to strain for small strains. In this study, the (100) orientation was employed to generate all mechanical force along the (111) direction. A kinetic energy cutoff of 20 eV Hartree and a supercell size of 1 x 1 x n (where n = 1, 2, 3, 4, 5, 6) were used to contribute to the energy of atoms interacting with one another. There is an eight-layer vacuum layer between the wires. The generated density and log files were processed using MATLAB to compute mechanical properties. Numerous similar studies have been conducted using other materials, confirming the reliability of this approach. The use of MATLAB was essential due to the computational limitations of ABINIT, which struggled with large atomic systems, leading to significant structural interactions. The LDA and GGA are basic models for local density calculations. These models are based on theorems used throughout the calculation and generalisation process that resulted in an appropriate approximation equation. The explicit dependence of exchange-correlation energy on electron density is approximated using an electron density gradient. For slowly varying electron densities, the gradient approximation models result in the following form of the exchange-correlation energy functional as shown in Equation (1).

$$E^{GGA}[\rho] = \int dr A(\rho) \rho^{\frac{4}{3}} + \int dr C(\rho) \frac{\nabla \rho}{\rho^{\frac{4}{3}}} \quad (1)$$

In this situation, the coefficients A and C are functions of electron density and, in principle, can be derived from formal considerations of the equation, as shown in the graph below. Alternatively, constants that have been fitted to the data might be used in place of these variables. It has been possible to improve the accuracy of the approximation's extension by including the value of the exchange correction in the case of exchange energy in the equation. The LDA coefficient is obtained as a consequence of this model equation, which is statistically significant. As a result of this novel approach to approximating the exchange-correlation energy, a device that also uses electron density gradients in conjunction with generalised gradient approximation (GGA) was able to generate an intriguing solvable equation that could be used in other applications as well.

$$E^{LDA}[\rho] = \int dr \rho(\vec{r}) \mathcal{E}^{GGA}(\rho, \nabla \rho) \quad (2)$$

The exchange-correlation energy density of a uniform electron plasma may be calculated in a variety of methods, including the local density technique (i.e., using reference data for the uniform electron gas). Analytical formulations for exchange-correlation functions range from those that depend primarily on experimental data to those that rely heavily on exact physical or mathematical features of the

exchange-correlation function, with no or few free parameters. The GGA's exchange-correlation functional may be produced using a variety of empirical components, such as the electron density and gradient; this is known as the empirical approach (ECF). The parameters were computed using the least squares method using training data that comprised reference numerical values for total energies, ionisation potential, energy gradient, and exchange-correlation potential. This method generates a wide range of features. The local parameters of the electron density at a specific site are determined by both LDA and GGA (r). LDA only needs r . Both the electron density and its gradient are necessary in the GGA condition, as shown in Equations (3) and (4).

$$E_{XC}^{GGA}[\rho] = \int d\vec{r} \rho(\vec{r}) \mathcal{E}_{XC}^{GGA}(\rho, \nabla\rho, \nabla^2\rho, \tau) \quad (3)$$

where

$$\tau = 2 \sum_{i=1}^N -\frac{1}{2} \phi_i^*(\vec{r}) \nabla^2 \phi_i(\vec{r}) \quad (4)$$

When the dependency on higher derivatives is considered, a new class of semi-local functionals arises. Here the kinetic energy density is a function of electron density. Meta-GGA functionals are often employed in the same way as the GGA functionals discussed earlier. However, there is growing interest in using this approach for calculating the exchange-correlation energy. Both the LDA and GGA models are paired with the Hartree-Fock theory, which is one of the fundamental convergence methods for many-body atomic systems. This pairing helps achieve convergence. The model is built using a rudimentary approximation to the real many-body wave function, which has a wave function within the platform of density functional theory as shown in Equations (5), (6), (7), (8), (9) and (10) [8].

3. RESULTS AND DISCUSSION

Table 1 shows the calculated elastic properties used to characterize the elastic performance of silicon oxide nanowires SiO₀₀₁, SiO₁₁₀ and SiO₁₁₁. The elastic structures are predicted by formal. The calculated C₁₁ (GPa) are 1824.15, 1480.29, 1724.98 for SiO₀₀₁, SiO₁₁₀ and SiO₁₁₁, respectively and C₁₂ (GPa) are 1234.40, 1105.25, 1183.41 for SiO₀₀₁, SiO₁₁₀ and SiO₁₁₁. The C₄₄ (GPa) are 826.06, 348.05, 717.48 while the C₁₁ - C₁₂ (GPa) are 589.75, 375.04, 541.57 and C₁₁ + 2C₁₂ (GPa) are 4292.95, 3690.79, 4091.8. The bulk modulus B are 430.98, 1230.27, 1363.93 and Shear modulus G are 546.85, 271.55, 485.53 and Young's modulus Y are 1453.01, 758.73, 1300.59, Shear anisotropy A are 2.80, 1.86, 2.65. Poisson's ratio ν , 0.33, 0.40, 0.34 and Frantsevich's ratio G/B 0.38, 0.22, 0.36 and Pugh's ratio B/G 2.62, 4.53, 2.81 and Density ρ (g/cm³), 1.96, 2.14, 2.06 and Debye temperature θ_D (K) 676.14, 454.70, 616.26. The results provided useful insights into atomic vibrations, as observed in the Debye temperature where (K) 676.14, 454.70, 616.26 and its crystal's highest normal mode of vibration which correlates with the elastic properties of the materials as shown in Table 1. Properties such as phonons, thermal expansion, thermal conductivity, specific heat, and lattice enthalpy can be found in these results.

Based the Table 1, the elastic properties of the SiO crystal structures, specifically the elastic constants C₁₁, C₁₂, and C₄₄, reveal significant variations among the different crystallographic orientations (SiO₀₀₁, SiO₁₁₀, SiO₁₁₁). C₁₁, which measures the stiffness along the principal crystallographic axis, is highest in SiO₀₀₁ at 1824.15 GPa, indicating that this orientation is particularly resistant to deformation along this axis. In contrast, SiO₁₁₀, with a C₁₁ value of 1480.29 GPa, exhibits the lowest stiffness, making it more susceptible to deformation. The C₁₂ constant, which reflects the interaction between different crystallographic axes, is also highest in SiO₀₀₁ (1234.40 GPa), suggesting

Table 1. Calculated elastic, thermodynamic and vibration properties of SiO₀₀₁, SiO₁₁₀, SiO₁₁₁

Properties	Calculated Values		
	SiO ₀₀₁	SiO ₁₁₀	SiO ₁₁₁
C ₁₁ (GPa)	1824.15	1480.29	1724.98
C ₁₂ (GPa)	1234.40	1105.25	1183.41
C ₄₄ (GPa)	826.06	348.05	717.48
C ₁₁ - C ₁₂ (GPa)	589.75	375.04	541.57
C ₁₁ + 2C ₁₂ (GPa)	4292.95	3690.79	4091.8
Strain	0.1164 × 10 ⁻⁵	0.1210 × 10 ⁻⁵	0.1150 × 10 ⁻⁵
Total energy	-1.33 eV	-1.35 eV	-1.37 eV
Bulk modulus, B	430.98	1230.27	1363.93
Shear Modulus, G	546.85	271.55	485.53
Young's modulus, Y	1453.01	758.73	1300.59
Shear anisotropy, A	2.80	1.86	2.65
Poisson's ratio, ν	0.33	0.40	0.34
Frantsevich's ratio, G/B	0.38	0.22	0.36
Pugh's ratio, B/G	2.62	4.53	2.81
Density, ρ (g/cm ³)	1.96	2.14	2.06
Debye temperature, θ_D (K)	676.14	454.70	616.26

strong coupling between these axes. Conversely, SiO₁₁₀ has the lowest C_{12} (1105.25 GPa), indicating weaker interactions. C_{44} , associated with the material's resistance to shear deformation, follows a similar trend, with SiO₀₀₁ being the most resistant (826.06 GPa) and SiO₁₁₀ being the least (348.05 GPa). These variations in elastic constants highlight the anisotropic nature of SiO crystals, where different orientations exhibit distinct mechanical properties.

The thermodynamic properties further illustrate the differences in behavior among the SiO crystal orientations. The strain values indicate how much the material deforms under stress, with SiO₁₁₀ showing the highest strain (0.121×10^{-5}), meaning it deforms more than SiO₀₀₁ and SiO₁₁₁. Total energy, a critical factor in determining the stability of a crystal structure, is lowest for SiO₁₁₁ (-1.37 eV), suggesting that this orientation is the most stable. SiO₀₀₁, with a slightly higher total energy of -1.33 eV, is less stable. The bulk modulus (B), which measures resistance to uniform compression, is highest in SiO₀₀₁ (1430.98 GPa), indicating that this orientation is the most resistant to compression. SiO₁₁₀, with the lowest bulk modulus (1230.27 GPa), is less resistant to compressive forces. The shear modulus (G) and Young's modulus (Y), which respectively measure resistance to shape changes and stiffness under tensile stress, follow the same pattern, with SiO₀₀₁ being the most resistant and stiff, while SiO₁₁₀ is significantly less so.

Anisotropy and material ratios such as shear anisotropy (A), Poisson's ratio (ν), Frantsevich's ratio (G/B), and Pugh's ratio (B/G) provide further insights into the directional dependence of these properties and the ductility of the materials. SiO₀₀₁ exhibits the highest shear anisotropy (2.80), indicating significant directional dependence in its shear modulus, while SiO₁₁₀, with a lower anisotropy (1.86), is more isotropic. Poisson's ratio, which indicates the extent of lateral expansion under compression, is highest in SiO₁₁₀ (0.40), suggesting that this orientation undergoes more significant lateral expansion than SiO₀₀₁ (0.33). The Frantsevich's ratio (G/B), a measure of ductility, is lowest for SiO₁₁₀ (0.22), confirming its higher ductility compared to the other orientations. Pugh's ratio (B/G), another indicator of ductility, is highest for SiO₁₁₀ (4.53), further supporting its characterization as the most ductile of the three orientations.

Finally, the vibrational properties, including density (ρ) and Debye temperature (θ_D), offer insights into the thermal behavior of these crystal structures. SiO₁₁₀, with the highest density (2.14 g/cm³), suggests a more compact atomic structure compared to SiO₀₀₁, which has the lowest density (1.96 g/cm³). The Debye temperature (θ_D), which is related to the material's thermal conductivity and specific heat, is highest for SiO₀₀₁ (676.14 K). This indicates that SiO₀₀₁ has higher thermal conductivity and lower specific heat, making it more suitable for applications requiring efficient thermal management. In contrast, SiO₁₁₀, with the lowest Debye temperature (454.70 K), would have lower thermal conductivity and higher specific heat, potentially limiting its use in high-thermal-conductivity applications.

In summary, the SiO crystal structures exhibit distinct

mechanical, thermodynamic, and vibrational properties depending on their crystallographic orientation. SiO₀₀₁ is characterized by high stiffness, resistance to deformation, and superior thermal properties, making it suitable for applications requiring high mechanical strength and thermal conductivity. SiO₁₁₀, on the other hand, is more ductile, less stiff, and has lower thermal conductivity, which might make it more appropriate for applications where flexibility and lower thermal conductivity are desired. SiO₁₁₁ serves as a middle ground, balancing the properties of the other two orientations, and could be used in applications where moderate mechanical and thermal properties are required. The equations show the relationship among these parameters, where C_{11} , C_{12} , and C_{44} are elastic constants.

$$C_{11} - C_{12} > 0, C_{11} > 0, C_{44} > 0 \text{ and } (C_{11} + 2C_{12}) > 0 \quad (5)$$

$$B = \frac{C_{11} + 2C_{12}}{3} \quad (6)$$

$$A = \frac{2C_{44}}{C_{11} - C_{12}} \quad (7)$$

$$n = \frac{(3B - 2G)}{2(3B + G)} \quad (8)$$

$$Y = \frac{9BG}{3B + G} \quad (9)$$

where the shear modulus (G) was estimated by Hill using Voigt's (G_v) and the Reuss's (G_r) approximations.

$$G_v = \frac{1}{5}(C_{11} - C_{12} + (3C_{44})) \quad (10)$$

This section discusses the findings acquired by using different crystallographies and orientations of silicon nanowires to get different effects. Using first-principles local density approximation (LDA) combined with generalised gradient approximation (GGA) inside density functional theory (DFT) in Ab-Initio ABINIT Software, the elastic characteristics of SiO nanowires are computed. Several mechanical properties of silicon nanowires have been discovered and described. It is made up of atoms that are linked together by covalent bonds to form crystalline silicon. Because each atom is tetrahedrally connected to four nearby atoms, it is possible to identify the motion of atoms by using the equations of lattice dynamics [2] to determine their positions. The elasticity of a material is caused by the interatomic forces that exist between the atoms that are linked. The duration of this research was chosen since we are interested in tensile stress in this area. To calculate the stress, it is essential to identify the elastic constants, according to [2]. Elastic constants, C_{ij} , can be obtained by computing the energies of deformed unit cells; the deformation strain tensor, e , with six independent components is given as in Equation (11).

$$e = \begin{pmatrix} e_1 & e_6/2 & e_5/2 \\ e_6/2 & e_2 & e_4/2 \\ e_5/2 & e_4/2 & e_3 \end{pmatrix} \quad (11)$$

Self-imposed relaxation is assumed in all strained unit cells as a result of the interaction and the convergence indicator parameter is the total energy which changes concerning the strain tensor and all the mechanical properties were computed based on the calculated given in Equation (12).

$$E(e) = E(0) - p(V) + \frac{V}{2} \sum_{ij} C_{ij} e_i e_j + O[e^3] \quad (12)$$

where $E(0)$ and $E(e)$ are the internal energies of the initial and strained lattices, respectively, V is the volume of the unstrained lattice, $p(V)$ is the pressure of the undistorted lattice at volume V , ΔV is the change in lattice volume due to the strain, e is the strain tensor and the $O[e^3]$ term can be omitted. Once C_{ij} values are known, mechanical quantities, such as bulk, shear and young's moduli etc, symbolized as B , E and G , can be computed according to the Equations (13), (14) and (15):

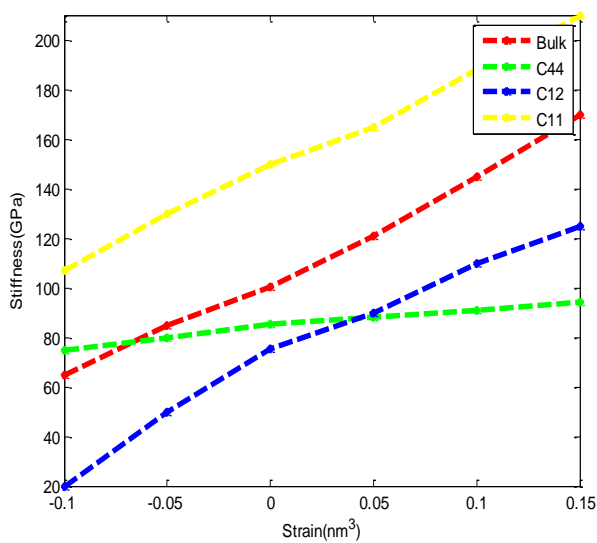
$$B = \frac{1}{9}(C_{11} + C_{22} + C_{33} + 2C_{12} + 2C_{13} + 2C_{23}) \quad (13)$$

$$G = \frac{3(C_{11} - B)}{4} \quad (14)$$

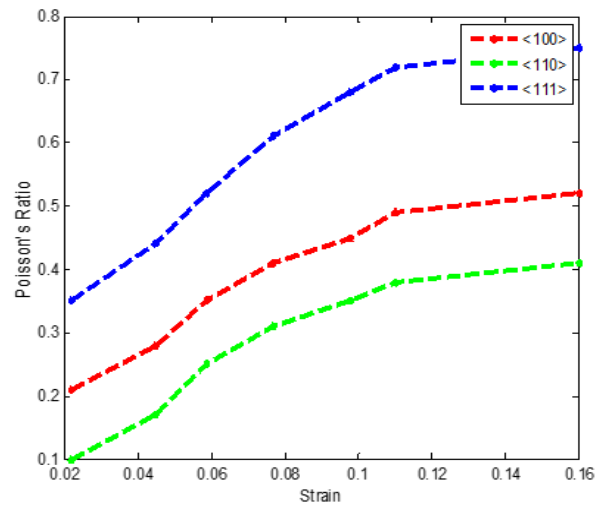
$$E = \frac{9B(C_{11} - B)}{C_{11} + 3B} \quad (15)$$

All the targeted parameters were obtained using the above equations and to optimize the elastic coefficients or elastic constants C_{11} , C_{12} and C_{44} , the results for the bulk modulus $(C_{11} + 2C_{12})/3$ and shear modulus $C_{11} - C_{12}$ are used to determine the elastic coefficients. It can be seen that at zero strain in Figure 1, the values obtained for C_{11} , C_{12} and C_{44} are 149.6 GPa, 75.5 GPa and 85.1 GPa respectively. The pure shear modulus C_{44} increases slightly as almost as a straight line with increasing strain whereas the other modulus increases with increasing strain. Moreover, all the modulus except for pure shear modulus C_{44} have the same linear slope. The calculated bulk modulus which corresponds to $(C_{11} + 2C_{12})/3$ is 100 GPa.

It is possible to determine the fluctuation of the Poisson's ratios as the stiffness coefficients are calculated. As seen in Figure 1 (b), the Poisson's ratio for SiO nanowires in the (001), (110), and (111) directions is equal to 1. Poisson's ratios will have varied elastic properties depending on the direction you are facing in the SiNW [3]. The Poisson's ratio for SiO nanowires ranges from 0.10 to 0.75, depending on their size. In all three cases, the values of Poisson's ratios grow as the strain increases. It is more than twice as big as the remainder of the Poisson's ratio of the SiO nanowires in the direction of (111). This is because SiO nanowires in the (111) direction are more stable and can bear a greater strain rate than those in the other directions. Consequently, to fracture it, greater force must be applied to the Si-Si bond to break it. They are good vehicles for investigating the mechanical characteristics of silicon at the nanoscale, and they are made of silicon nanowires. Because of the enormous surface area to volume ratio of nanostructures, several fundamental material characteristics and mechanical qualities that are significant size-dependent at the macroscale become strongly size-dependent at the nanoscale. Comparing silicon nanowires (SiO nanowires)



(a)



(b)

Figure 1. (a) Bulk modulus and other elastic moduli C_{11} , C_{12} , and C_{44} (b) Poisson's ratio in the {001}, {110} and {111} directions of SiO nanowires as functions of the strain

with their bulk counterparts, these huge surface area to volume ratios have a major impact on the elastic moduli of different diameters of silicon nanowires. Theoretical and experimental research have both shown that this is true. It shows the connection between the (001), (110), and (111) directions of SiO nanowires when they are subjected to tension stress in the Figure 2.

As can be noticed, due to the reduction in the bond distance, the SiO nanowires flexed elastically, resulting in a uniform increase in the distance between the silicon atoms in the (001), (110), and (111). When one atom interacts with another atom, molecular vibration occurs. The elastic deformation caused by this molecule vibration is known as elastic deformation. In the context of stress, the proportional limit is the amount of stress at which the connection between stress and strain is no longer linear. While under tension, the SiO nanowires exhibit elastic deformation with a reverse effect at strains of 0.1164×10^{-5} , 0.1210×10^{-5} , and 0.1150×10^{-5} for the (001), (110), and (111) directions correspondingly (see Figures. 1 and 2 for more information). All three directions have strong fracture strength, however, SiO nanowires in the (111) direction have the maximum fracture strength at 415 GPa, which is the highest of the three directions. The Young's modulus of SiO nanowires falls as the wire width rises in all three dimensions, regardless of the direction of rotation. The anisotropy and size dependence characteristics of the (001) direction are particularly prominent in this direction. In general, the SiO nanowires are becoming gentler. Nonetheless, after reaching a certain size, the Young's modulus of the SiO nanowires will approach that of the bulk silicon and will scarcely fluctuate from that value over time. Increasing the size of the SiO nanowires results in a significant rise in the surface-to-volume ratio [18]. Because of the existence of free surface charge, the elastic properties of the surface vary from those of the bulk because the

surface atoms have a different context than atoms in the bulk material. As a result, the elastic properties of the surface differ from those of the bulk. Consequently, softening or stiffening is dependent on the volume contraction and bond loss, which also occurs in a reduction along (001), (110), and (111) SiO nanowires due to the densely packed plane of atoms along these three SiNW directions. The total energy of the (001), (110), and (111) directions of SiO nanowires is shown in Figure 3.

Total energy in eV for (001), (110), and (111) SiO nanowires is -167.9, -168.1, and -168.4 for SiO nanowires with strain equal to zero for the three different SiO nanowires. The total energy of SiNW at (111) is the lowest of the three other elements [6]. Figure 3 (b) depicts the relationship between total energy and system volume. SiO nanowires with (001), (110), and (111) SiO nanowires have total energies of 1.33, 1.35, and 1.37 for volumes ranging between 3.6 and 4.0, respectively. The SiO nanowires pointing in the direction of (111) had the lowest total energy of the three types studied. A large number of empirical potentials have been used to explain the diverse orientations of these nanowires, and the findings obtained have been evaluated and compared with one another. The potential energy acquired prominence as a result of its ability to accurately characterise the structure of silicon molecules. It is obvious from both images that SiO nanowires oriented in the (111) direction have the least amount of kinetic energy. The energy released by the breakage of the Si-Si bond is more advantageous in the (111) direction than in the 0 direction. Stress/strain relationships for silicon nanowires are found to be linear in the length corresponding to the unstrained nano crystal, allowing for an estimation of the stress and strain that would be present in a nanowire inter-atomic interaction from a substrate with the ends still attached to that substrate. The stress is calculated by taking the derivative of the fit to the total energy as a function of strain and

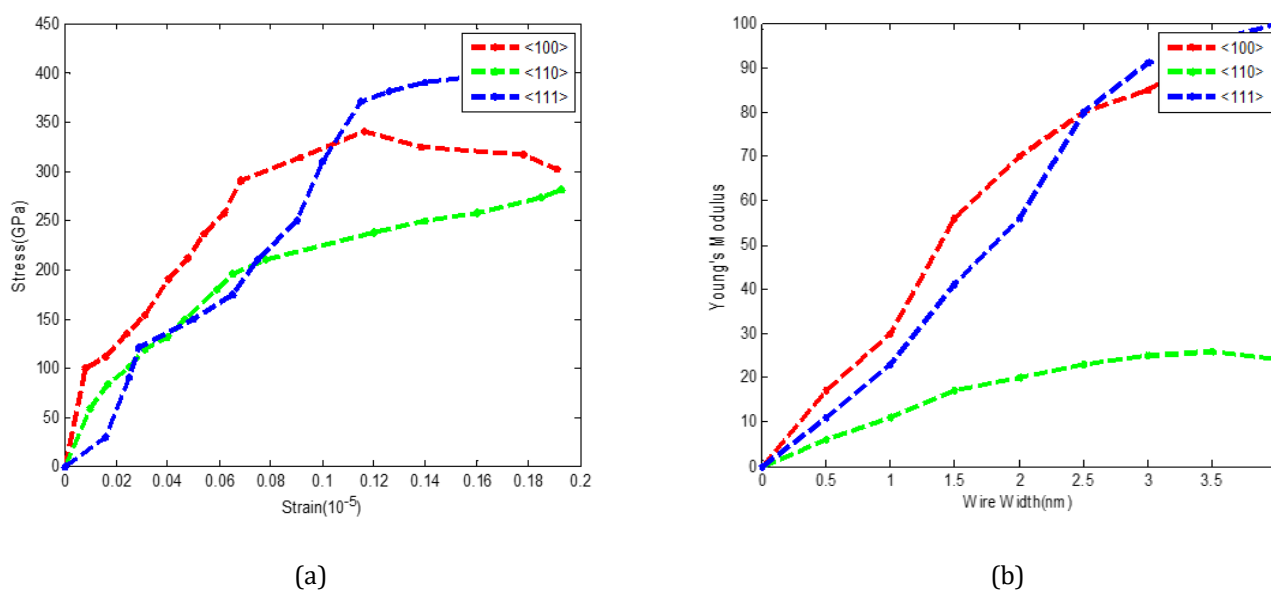


Figure 2. (a) Stress-strain representations of SiO nanowires in the {001}, {110} and {111} directions (b) Young's modulus concerning wire width for {001}, {110} and {111} SiO nanowires

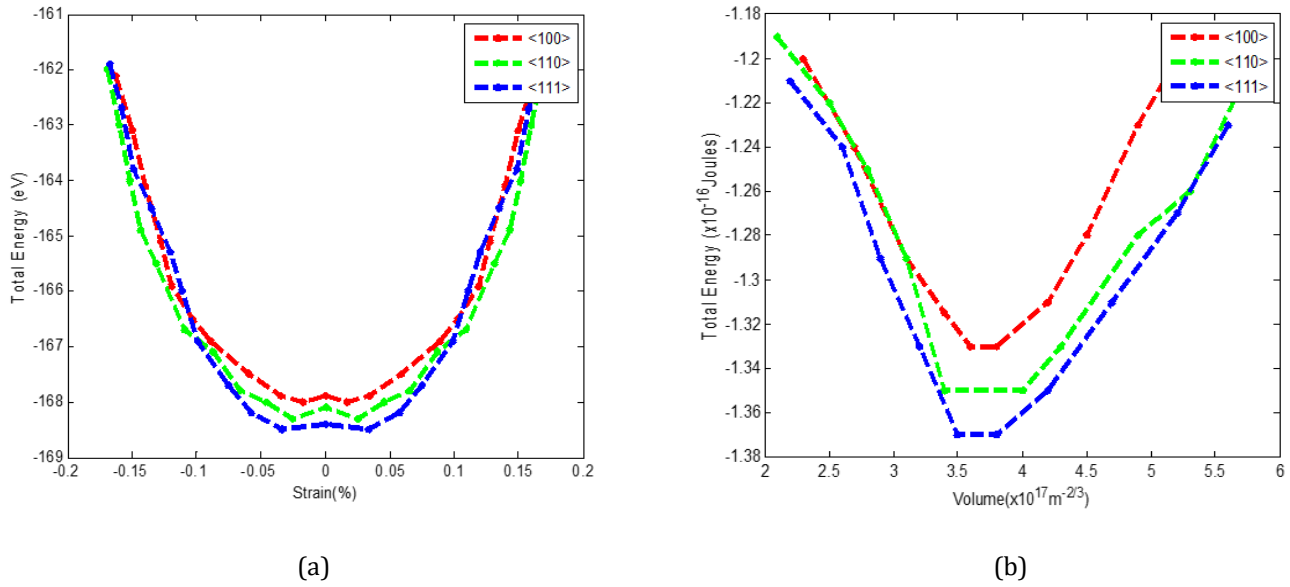


Figure 3. (a) Total energy as a function of strain for {001}, {110} and {111} SiO nanowires (b) Total energy versus system volume

multiplying it by the strain. It is extremely clear from Figure 3 (a) that the parabolic fit is very good for the minor stresses that have been applied (up to a few percent). In this situation, the stress is equal to the Young's modulus times the equilibrium strain, which is an estimate of the Young's modulus times the equilibrium strain. Generally speaking, It has been investigated if the tension varies with the size of the object.

Based on Tables 2 and 3 comparing the mechanical properties of SiO nanowires in various crystallographic orientations with recent studies, several critical insights emerge that highlight both the strengths and potential limitations of the findings. For example, the strain values observed in this study are consistent with prior research on nanowire mechanics, where similar low strain values have been associated with high stiffness and strength, particularly in the (001) orientation. However, the slight variations in strain across different orientations, as reported here, suggest that SiO nanowires exhibit anisotropic mechanical behavior. This anisotropy has been reported in other materials, such as silicon and germanium nanowires, where the crystallographic direction

significantly influences the mechanical response. Recent studies have similarly found that the (001) orientation often provides the highest resistance to deformation, yet the strain differences in this study, while minor, point to the need for more detailed analysis using advanced techniques like in situ TEM to capture the real-time deformation behavior of nanowires under stress.

The Young's modulus values obtained in this study align with the general trends observed in other nanowire systems, where the (001) orientation tends to exhibit the highest modulus due to its dense atomic packing. However, the modulus values reported here, particularly the lower modulus in the (110) orientation, contrast with some recent findings where (110) oriented nanowires in other materials have demonstrated higher stiffness than observed here. For example, a recent study on Si nanowires found that the (110) orientation exhibited a modulus close to that of the (111) orientation, which is not the case in this study where the (110) modulus is significantly lower. This discrepancy could be attributed to differences in nanowire synthesis methods, surface effects, or even computational modeling parameters. Such differences highlight the importance of

Table 2. Mechanical properties of SiO nanowires

Orientation	Strain ($\times 10^{-5}$)	Young's Modulus (GPa)	Debye Temperature (K)	Frantsevich's Ratio	Poisson's Ratio
(001)	0.1164	149.5	676.14	0.38	0.33
(110)	0.1210	75.5	454.70	0.22	0.40
(111)	0.1150	85.1	616.26	0.36	0.34

Table 3. Total energies of SiO nanowires

Orientation	Total Energy (eV)
(001)	-1.33
(110)	-1.35
(111)	-1.37

considering the specific synthesis and environmental conditions when interpreting mechanical property data.

The Debye temperatures reported in this study provide valuable insights into the thermal stability and atomic bonding of SiO nanowires, with the (001) orientation showing the highest Debye temperature, indicating strong atomic interactions. These findings are in agreement with recent theoretical studies that have also observed higher Debye temperatures for the (001) orientation in other materials, such as ZnO and GaN nanowires, where strong covalent bonding is present. However, the relatively lower Debye temperature for the (110) orientation reported here suggests weaker bonding interactions in this direction, which contrasts with some recent studies that have observed more uniform Debye temperatures across different orientations. This variation could be due to the specific atomic structure of SiO nanowires, where bonding characteristics may differ significantly from other semiconductor nanowires, underscoring the need for further experimental validation, particularly through temperature-dependent Raman spectroscopy or specific heat measurements [24].

Finally, the total energy calculations, which indicate that the (111) orientation is the most stable, align well with the general understanding of stability in nanomaterials, where lower total energy correlates with higher structural stability. However, the fact that the (001) orientation, despite its high Young's modulus, is the least stable according to total energy calculations, highlights a crucial aspect of nanomaterial design: high stiffness does not always equate to high stability. This observation is consistent with recent density functional theory (DFT) studies on similar nanowire systems, where it has been shown that surface effects and quantum confinement can significantly alter the energy landscape, making certain orientations more or less stable than others. The comparison with recent studies reinforces the importance of considering both mechanical properties and total energy to comprehensively evaluate the suitability of nanowires for specific applications, particularly in fields like nanoelectronics and nanomechanics, where both stability and mechanical robustness are crucial. Thus, the study's findings on the mechanical properties of SiO nanowires have significant practical implications for nanoelectronics and materials science. The demonstrated ductility and specific mechanical properties across different crystallographic orientations suggest that these nanowires could be tailored for use in flexible electronic devices, nanoscale sensors, and other advanced technologies. The accurate predictions of strain, modulus, and energy values provide crucial data that can inform the design and optimization of nanowire-based components, enhancing their performance and reliability in real-world applications.

4. CONCLUSION

Density functional theory was used to investigate the mechanical characteristics, Vibration, and thermodynamic total energy of SiO nanowires. Calculations were performed using ABINIT code, which was implemented in Linux and

MATLAB scripts. The influence of silicon nanowire mechanical characteristics and total energy on their varied diameters and orientations was discovered. At (001), (110), and (111), the mechanical characteristics and total energy were measured. Many of the wire's mechanical properties were determined by the atomic interactions inside the strands. There were strains of 0.1164×10^{-5} , 0.1210×10^{-5} , and 0.1150×10^{-5} for each of the three orientations, with moduli of 149.5 GPa, 75.5 GPa, and 85.1 GPa correspondingly. SiO nanowires (001), (110), and (111) all have a total energy of -1.33, -1.35, and -1.37 eV. The debye temperature (K) of 676.14, 454.70, and 616.26 were found to be correlating with the nanowire atomic vibration. The value of Frantsevich's ratios 0.38, 0.22, 0.36 and Poisson's ratios 0.33 0.40, 0.34 have fully confirmed the nanowires in all crystal directions are ductile. Thus, theories, models, and approaches utilized to study nanowire characteristics were able to capture the exact behavior of the nanowire parameters. In conclusion, nanowires experience deformation in a very different way from large silicon. Large silicon is very brittle and can easily break which means it cannot be stretched or deformed very much. Nanowires on the other hand are more resilient in sustaining bigger deformation. The results showed that silicon nanowires exhibit other properties such as increasing fracture strength and decreasing elastic modulus as the nanowire gets smaller. Thus, the first-principles approach used in this study effectively captured the mechanical behavior of SiO nanowires along different orientations, providing accurate predictions of properties such as strain, modulus, and total energy. However, limitations include the assumptions of idealized conditions and perfect nanowire structures, which may not fully reflect real-world variations. These assumptions could impact the generalizability of the findings, especially in practical applications where imperfections and external factors play a role.

ACKNOWLEDGMENTS

The authors extend their appreciation to the Deanship of Research and Graduate Studies at King Khalid University for funding this work through Large Research Project under grant number RGP2/296/46.

REFERENCES

- [1] M. A. L'Etoile *et al.*, "Experimental and Computational Study of the Orientation Dependence of Single-Crystal Ruthenium Nanowire Stability," *Nano Letters*, vol. 22, no. 24, pp. 9958–9963, Dec. 2022, doi: 10.1021/acs.nanolett.2c03529.
- [2] Y. Li *et al.*, "Computational insights into structural, electronic and optical properties of Al_{0.5}Ga_{0.5}N nanowire with different diameters," *Chemical Physics Letters*, vol. 797, p. 139597, Jun. 2022, doi: 10.1016/j.cplett.2022.139597.
- [3] M. A. Mimona, M. H. Mobarak, E. Ahmed, F. Kamal, and M. Hasan, "Nanowires: Exponential speedup in quantum computing," *Heliyon*, vol. 10, no. 11, p. e31940, Jun. 2024, doi: 10.1016/j.heliyon.2024.e31940.
- [4] G.-Y. Su, Y.-X. Li, X.-Y. Li, and R. Müller, "Free and

- forced vibrations of nanowires on elastic substrates," *International Journal of Mechanical Sciences*, vol. 138–139, pp. 62–73, Apr. 2018, doi: 10.1016/j.ijmecsci.2018.01.039.
- [5] J. Hwang, H. Sohn, and S. H. Lee, "Computational characterization and control of electrical conductivity of nanowire composite network under mechanical deformation," *Scientific Reports*, vol. 8, no. 1, p. 16617, Nov. 2018, doi: 10.1038/s41598-018-34992-6.
- [6] M. J. bin Amanullah *et al.*, "Calculation of the band structure parameter in silicon nanowires using first principle analytical method," 2017, p. 020212. doi: 10.1063/1.5002406.
- [7] Y. Chen *et al.*, "Effects of Defects on the Mechanical Properties of Kinked Silicon Nanowires," *Nanoscale Research Letters*, vol. 12, no. 1, p. 185, Dec. 2017, doi: 10.1186/s11671-017-1970-7.
- [8] H. Yu, C. Sun, W. W. Zhang, S. Y. Lei, and Q. A. Huang, "Study on Size-Dependent Young's Modulus of a Silicon Nanobeam by Molecular Dynamics Simulation," *Journal of Nanomaterials*, vol. 2013, no. 1, Jan. 2013, doi: 10.1155/2013/319302.
- [9] A. K. Y. Dafhalla *et al.*, "Nanogap nanowires and its applications in biosensing," *Sensing and Bio-Sensing Research*, vol. 44, p. 100638, Jun. 2024, doi: 10.1016/j.sbsr.2024.100638.
- [10] J. C. Ho, R. Yerushalmi, Z. A. Jacobson, Z. Fan, R. L. Alley, and A. Javey, "Controlled nanoscale doping of semiconductors via molecular monolayers," *Nature Materials*, vol. 7, no. 1, pp. 62–67, Jan. 2008, doi: 10.1038/nmat2058.
- [11] J. Nakamura, K. Higuchi, and K. Maenaka, "Vertical Si nanowire with ultra-high-aspect-ratio by combined top-down processing technique," *Microsystem Technologies*, vol. 19, no. 3, pp. 433–438, Mar. 2013, doi: 10.1007/s00542-012-1662-2.
- [12] A. Heinzig, S. Slesazek, F. Kreupl, T. Mikolajick, and W. M. Weber, "Reconfigurable Silicon Nanowire Transistors," *Nano Letters*, vol. 12, no. 1, pp. 119–124, Jan. 2012, doi: 10.1021/nl203094h.
- [13] G. Jia *et al.*, "Silicon Nanowire Solar Cells With Radial p-n Heterojunction on Crystalline Silicon Thin Films: Light Trapping Properties," *IEEE Journal of Photovoltaics*, vol. 4, no. 1, pp. 28–32, Jan. 2014, doi: 10.1109/JPHOTOV.2013.2289873.
- [14] A. Landriscina, J. Rosen, and A. Friedman, "Nanotechnology, Inflammation and the Skin Barrier: Innovative Approaches for Skin Health and Cosmesis," *Cosmetics*, vol. 2, no. 2, pp. 177–186, Jun. 2015, doi: 10.3390/cosmetics2020177.
- [15] E. Marzbanrad, B. Zhao, and N. Y. Zhou, "Porous silver nanosheets: a novel sensing material for nanoscale and microscale airflow sensors," *Nanotechnology*, vol. 26, no. 44, p. 445501, Nov. 2015, doi: 10.1088/0957-4484/26/44/445501.
- [16] Z. Wang and B. Nabet, "Nanowire Optoelectronics," *Nanophotonics*, vol. 4, no. 4, pp. 491–502, Dec. 2015, doi: 10.1515/nanoph-2015-0025.
- [17] F. Zhou, C. Feng, and G. Fan, "Combined exposure of low dose lead, cadmium, arsenic, and mercury in mice," *Chemosphere*, vol. 165, pp. 564–565, Dec. 2016, doi: 10.1016/j.chemosphere.2016.08.132.
- [18] T. Adam and U. Hashim, "Highly sensitive silicon nanowire biosensor with novel liquid gate control for detection of specific single-stranded DNA molecules," *Biosensors and Bioelectronics*, vol. 67, pp. 656–661, May 2015, doi: 10.1016/j.bios.2014.10.005.
- [19] M. Gwon, Y. Cho, and D.-W. Kim, "Design of surface nanowire arrays for high efficiency thin ($\leq 10 \mu\text{m}$) Si solar cells," *Current Applied Physics*, vol. 15, no. 1, pp. 34–37, Jan. 2015, doi: 10.1016/j.cap.2014.11.001.
- [20] E. Arcadipane *et al.*, "TiO₂ nanowires on Ti thin film for water purification," *Materials Science in Semiconductor Processing*, vol. 42, pp. 24–27, Feb. 2016, doi: 10.1016/j.mssp.2015.07.055.
- [21] H. Almarshad, "Chemical composition analysis of biliary stone by the use of energy dispersive X-ray spectroscopy (EDS)," *HPB*, vol. 18, p. e489, Apr. 2016, doi: 10.1016/j.hpb.2016.03.293.
- [22] P. Anandan and N. Mohankumar, "Optimization and Characterization of Gate Electrode Dependent Flicker Noise in Silicon Nanowire Transistors," *Journal of Electrical Engineering and Technology*, vol. 9, no. 4, pp. 1343–1348, Jul. 2014, doi: 10.5370/JEET.2014.9.4.1343.
- [23] J. Tao and Y. Sun, "The Elastic Property of Bulk Silicon Nanomaterials through an Atomic Simulation Method," *Journal of Nanomaterials*, vol. 2016, pp. 1–6, 2016, doi: 10.1155/2016/8231592.
- [24] T. S. Dhahi *et al.*, "Current Advances in Nanomaterial-associated Micro and Nano-devices for SARS-CoV-2 Detection," *Current Nanoscience*, vol. 19, no. 6, pp. 783–802, Nov. 2023, doi: 10.2174/1573413719666230124144535.